

Experimental Testing of Elastic Properties of LayWood Pyramidal Cores

Michał Maslej* and Jerzy Smardzewski

Sandwich panels most commonly used in the furniture industry are layered structures composed of a hexagonal cell paper core. The use of wood-based composites in modelling truss and pyramidal cores of layered furniture panels is rather scarce. The effect of geometry in the auxetic truss core on the mechanical properties of manufactured wood-based materials was primarily explored in this study. Moreover, the need to conduct further studies was also stressed to determine the elastic properties of cells and cores manufactured from wood filaments using 3D printing. The aim of this study was to determine the effect of the type of filament used in 3D printing and the geometry of pyramidal core cells on elastic constants in cores with identical relative density. This paper presented analytical models of manufactured cells, results of numerical calculations performed using the finite element method, as well as experimental tests determining elastic constants of the cores. Digital image analysis was used and showed that cell geometry had a considerable effect on elastic properties of the core while maintaining identical relative density of these structures. The angle of cell arms had a particularly marked effect on these properties.

Keywords: Pyramidal cells; LayWood; Experiment; FEM

Contact information: Department of Furniture Design, Faculty of Wood Technology, Poznan University of Life Sciences, Poland; *Corresponding author: michal.maslej@up.poznan.pl

INTRODUCTION

The basic structural elements consisting of core and facings in layered sandwich panels are typically made from materials of high density and moduli of linear elasticity. Cores are usually composed of hexagonal, pyramidal, and truss cells or are constructed in the shell form (Wadley *et al.* 2003). The main materials used in their manufacture include aluminum, titanium, stainless steel (Alderson and Alderson 2007; Balawi and Abot 2008; Chen and Yan 2012), copper (He *et al.* 2017), polymers (Yin *et al.* 2013), carbon fibers (Finnegan *et al.* 2007; Wang *et al.* 2010), paper (Sam-Brew *et al.* 2011), and wood fibers (Smardzewski 2015). The density and mechanical properties of panels are also modified with a change in the core cell shape. For this reason designed cells need to have a comparable or identical relative density to avoid the effect of the amount of material used to construct the core on the rigidity in sandwich panels (Chen and Yan 2012; Schneider *et al.* 2015; Smardzewski 2015). In the furniture industry, the most commonly used sandwich panels are lightweight furniture panels comprising of a paper core with hexagonal cells. However, the results from various studies (Barboutis and Vassiliou 2005; Smardzewski and Prekrat 2012; Smardzewski 2013, 2015) have revealed that these panels are characterized by low rigidity and bending strength. To date, the research conducted has also shown that changes in geometry and dimensions of hexagonal cells of the core have a major effect on the rigidity of furniture panels (Voth and Yadama 2010; Majewski and Smardzewski 2012, 2015; Smardzewski and Prekrat 2012; Smardzewski 2013). Attempts

have also been made to replace paper cores with hexagonal cells using a wavy core manufactured from wood fibers (Smardzewski and Majewski 2015; Smardzewski and Jasińska 2016), interlocking bands of plywood and high-density fiberboard (HDF) (Klimek *et al.* 2016), truss, and pyramidal structures typically manufactured from tin or glass or carbon fiber composites (Voth and Yadama 2010; Yin *et al.* 2011, 2013; Yang *et al.* 2015; Imbalzano *et al.* 2016). Wood materials have been rarely used to model truss, auxetic, and pyramidal structures. The primary aim of those attempts was to determine the elastic properties of the obtained periodic systems. In turn, numerical calculations were used to determine the effect of auxetic truss cell geometry in the core on the mechanical properties of layered wood-based panels (Wojnowska *et al.* 2017; Peliński and Smardzewski 2019). Those studies showed potentially advantageous elastic properties of those structures, thus suggesting their future applicability.

In contrast, few reports have considered the application of 3D printing technology using biocomposites to manufacture complex pyramidal structures in cores of layered furniture panels (Smardzewski *et al.* 2018). This is noteworthy, because layered panels made from wood and wood-based materials are an excellent alternative for comparable composites manufactured from metals or plastics (Xiong *et al.* 2010; Gao *et al.* 2013). They are lighter and in relation to their density they are stronger and more rigid. This facilitates efficient management of natural resources, because they are derived from renewable materials. Moreover, the applications of pyramidal structures manufactured by 3D printing from LayWood filaments are highly promising (Smardzewski and Wojciechowski 2019), and thus one of the reasons why the present study was undertaken.

The aim of this study was to determine the effect of the type of filament used in 3D printing and the geometry of pyramidal core cells on the elastic constants of the cores with identical relative density. This paper presents analytical models of manufactured cells, results of numerical calculations using the finite element method (FEM), as well as experimental results of tests for determining the elastic constants of the core.

EXPERIMENTAL

Mathematical Models

Figure 1 presents a computational model of the investigated pyramidal cell. Analysis of this geometry shows that it is composed of two perpendicular arms. The variables are as follows: L_x and L_y (mm) are the length of cells in the X and Y directions, respectively, l_x and l_y (mm) are the length of cell ribs in the X and Y directions, respectively, h (mm) is the cell height, φ_x and φ_y ($^\circ$) are the rib angle in the ZX and ZY planes, respectively, $2a = s$ (mm) is the width of rib base, and t (mm) is the rib thickness. To date, the results of research conducted on similar structures have shown that the mechanical properties of panels with cell cores are considerably influenced by the length and angle of cell ribs, dimensions of rib cross-section, and the type of material from which they were manufactured, and thus also their relative density (Loinsigh *et al.* 2012; Gao *et al.* 2013; Zhang *et al.* 2013; Che *et al.* 2014; Jin *et al.* 2015; Zhong *et al.* 2015; Smardzewski *et al.* 2018). For this reason, it was decided to first determine the relative density of the modelled core cells.

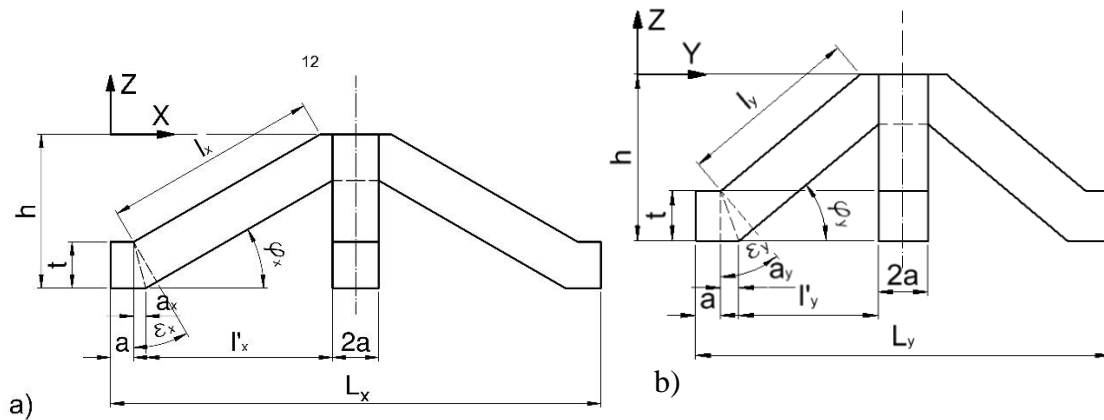


Fig. 1. Elementary section of rib geometry, projection on a) ZX and b) ZY planes

Relative density (ρ) of the analyzed structure may be described as,

$$\rho = \frac{V_{s(ZX)} + V_{s(ZY)}}{L_x L_y h} \tag{1}$$

where $V_{s(ZX)}$ (mm^3) is the volume of rib in the ZX plane and $V_{s(ZY)}$ (mm^3) is the volume of rib in the ZY plane:

$$V_{s(ZX)} = s \left(h L_x - 4(h - t) \left(a + \frac{1}{2} l'_x \right) \right) \tag{2}$$

$$V_{s(ZY)} = s \left(h L_y - 4(h - t) \left(a + \frac{1}{2} l'_y \right) \right) - a^2 t \tag{3}$$

$$l'_x = (h - t) ctg \varphi_x \tag{4}$$

$$l'_y = (h - t) ctg \varphi_y \tag{5}$$

In view of the varied lengths of the cell ribs ($l_x > l_y$) (mm), using the diagram in Fig. 2, two moduli of linear elasticity E_x and E_y , and modulus of elasticity in shear G_{xy} were determined. Calculations were made applying the Maxwell-Mohr virtual force method (Wojnowska *et al.* 2017).

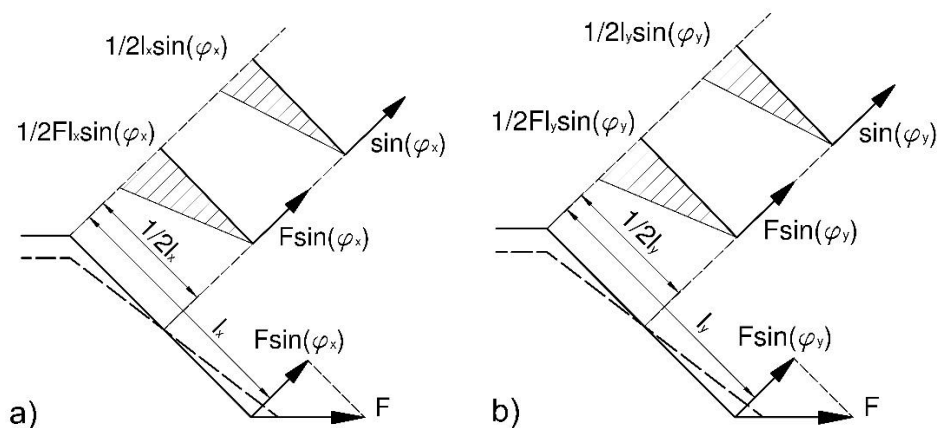


Fig. 2. Diagram of loading for a rib in the elementary core section

To determine the modulus (E_x), it was assumed that normal stress (σ_x , MPa) in the X direction is estimated using Eq. 6,

$$\sigma_x = \frac{F}{2ah} = E_x \frac{\Delta_x}{L_x} \quad (6)$$

where F (N) is the rib loading and Δ_x (mm) is the elongation caused by the action of force (F , N) (Fig. 2a). The elongation (Δ_x , mm) was calculated from Eq. 7,

$$\Delta_x = 4 \int_0^{l_x} \frac{M\bar{M}}{E_s J} dx \quad (7)$$

where E_s (MPa) is the modulus of elasticity for core substance, $M = 1/2Fl_{(x \text{ or } y)} \sin \varphi_{(x \text{ or } y)}$ (Nm) is the bending moment of rib, $\bar{M} = 1/2l_{(x \text{ or } y)} \sin \varphi_{(x \text{ or } y)}$ (Nm) is the virtual bending moment of rib, and J (m⁴) is the moment of inertia of rib cross-section given by Eq. 8 as:

$$J = \frac{2at^3}{12}, \quad (8)$$

thus:

$$\Delta_x = \frac{1}{E_s at^3} Fl_x^3 \sin^2(\varphi_x) \quad (9)$$

By solving the system of Eq. 10:

$$\left\{ \begin{array}{l} \frac{F}{2ah} = E_x \frac{\Delta_x}{L_x} \\ \Delta_x = \frac{1}{E_s at^3} Fl_x^3 \sin^2(\varphi_x) \end{array} \right\}, \quad (10)$$

the authors obtained Eq. 11 as follows:

$$E_x = \frac{E_s t^3 \left(2a + t \cdot tg\left(\frac{\varphi_x}{2}\right) + (h-t)ctg(\varphi_x) \right) \sin(\varphi_x)}{h(h-t)^3} \quad (11)$$

When determining the modulus (E_y , MPa) it was assumed that normal stress (σ_y , MPa) in the Y direction is,

$$\sigma_y = \frac{F}{2ah} = E_y \frac{\Delta_y}{L_y} \quad (12)$$

where Δ_y (mm) is the elongation caused by the action of F (N) (Fig. 2b). Elongation (Δ_y , mm) was calculated from Eq. 13 as,

$$\Delta_y = 4 \int_0^{l_y} \frac{M\bar{M}}{E_s J} dy \quad (13)$$

thus:

$$\Delta_y = \frac{1}{E_s at^3} Fl_y^3 \sin^2(\varphi_y) \quad (14)$$

By solving the system of Eq. 15,

$$\left\{ \begin{array}{l} \frac{F}{2ah} = E_y \frac{\Delta_y}{L_y} \\ \Delta_y = \frac{1}{E_s at^3} Fl_y^3 \sin^2(\varphi_y) \end{array} \right\} \quad (15)$$

the authors obtained Eq. 16 as:

$$E_y = \frac{E_s t^3 \left(2a + t \cdot \operatorname{tg}\left(\frac{\varphi_y}{2}\right) + (h-t) \operatorname{ctg}(\varphi_y) \right) \sin(\varphi_y)}{h(h-t)^3} \quad (16)$$

Due to the theoretical lack of transverse strain of ribs, Poisson's ratios ν_{xy} and ν_{yx} take the value of zero. In turn, the equation for the shear modulus of elasticity may be presented as Eq. 17:

$$G_{yx} = \frac{E_s t^3 \left(2a + t \cdot \operatorname{tg}\left(\frac{\varphi_y}{2}\right) + (h-t) \operatorname{ctg}(\varphi_y) \right) \sin(\varphi_y)}{2h(h-t)^3} \quad (17)$$

Filaments

Core cells were manufactured from filaments used in 3D printing technology applying fused deposition modelling (FDM). The selected filaments containing wood dust are commercially available as 3Dbamboo (LayWood 30%, LY), 3Dwood (LayWood 40%, LB), and polyactide (PLA) (PRI-MAT 3D; Filament Prima, Tarnowo Podgórze, Poland). PLA is the most popular resin for 3D printing because it is easy to use and has almost no odor. It adheres well to masking tape without requiring a heated printing bed or noxious solvents. LayWood contains 30 % or 40 % recycled wood dust and harmless binders made by co-polyesters. Elastic properties of these materials, *i.e.*, modulus of linear elasticity (E_s), modulus of rupture (MOR, MPa), and Poisson's ratio (ν), were determined in the uniaxial tension test. For each filament, a total of 10 dumbbell samples were prepared with the shape and dimensions as in Fig. 3. Tests were conducted according to the PN-EN ISO 527-3 (1998) standard using a Zwick 1445 universal strength testing machine (Zwick GmbH, Ulm, Germany) and a Dantec dynamics optical extensimeter system (Dantec Dynamics A/S, Skovlunde, Denmark). Table 1 presents the mean values and standard deviations (in parentheses) for the elastic constants of used filaments.

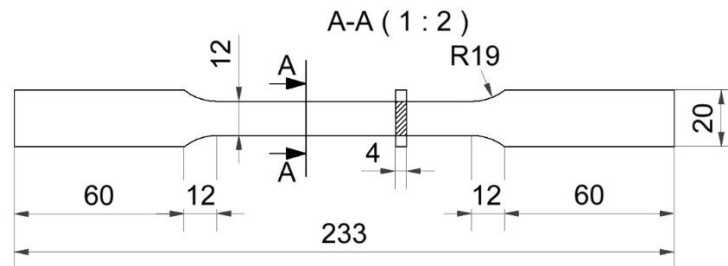


Fig. 3. Dimensions of dumbbell sample for uniaxial tension tests, units in mm

Table 1. Elastic Properties of Filaments

Material Type	Material Symbol	E_y	E_x	MOR _y	MOR _x	ν_{xy}	ν_{yx}
		(MPa)				-	
PLA	PLA	1842 (285)	-	17.11 (0.54)	-	0.48 (0.12)	
LayWood 40%	LB	458 (69)	-	11.68 (0.46)	-	0.26 (0.07)	
LayWood 30%	LY	1008 (266)	-	12.87 (0.41)	-	0.27 (0.06)	

Shapes of Core Cells

Based on the developed mathematical models and calculated elasticity constants for the core substance, eight types of pyramidal cells were computed, heuristically selected, and characterized by comparable relative density, but differed in shape and dimensions (Fig. 4). Cell A is a reference object, characterized by rib angle $\varphi_x = \varphi_y = 45^\circ$. Table 2 presents the most important dimensions and values of elastic constants calculated for the selected cells. At this stage, it was assumed that cells were manufactured from PLA. In the next step, cell shape was optimized using the Monte Carlo method, consisting in random search through the admissible area, and on the basis of obtained results the optimal value was estimated. The aim of that step was to produce cells noticeably differing from those heuristically identified and exhibiting extreme properties. The mathematical model for the optimization of rib cells included:

- a) Decision variables, for which the block of variables K_z takes the form,

$$K_z = \{\bar{x} = (x_1 \dots x_3): x_{i(\min)} \leq x_i \leq x_{i(\max)}: i = 1 \dots 3\} \quad (18)$$

where i is the the number of decision variables for cells, $x_1 = t = 2a$ (mm), $x_2 = \varphi_x$ ($^\circ$) is the angle of cell ribs in the ZX plane, and $x_3 = \varphi_y$ ($^\circ$) is the angle of cell walls in the ZY plane:

- b) Parameter E_s constituting the modulus of linear elasticity (MPa) for the material, from which ribs were manufactured, and
 c) Set of admissible values Φ is composed of inequality bounds $\Phi_i(x) > 0$, i.e.:

$$\Phi = \{\bar{x} = (x_1 \dots x_3): \Phi_i(\bar{x}) > 0: i = 1 \dots 3\} \quad (19)$$

The objective function was assumed to consist in the minimization of relative density of cells $\rho \rightarrow \min$ as well as maximization of values of moduli of linear elasticity of cells in the main orthotropic directions:

$$E_x \rightarrow \max, E_y \rightarrow \max \quad (20)$$

When attempting at optimization, it is necessary to provide minimal, intuitively estimated values of cell dimensions t_{\min} (mm), $\varphi_{x(\min)}$, $\varphi_{y(\min)}$ ($^\circ$), and maximal dimensions t_{\max} (mm), $\varphi_{x(\max)}$, and $\varphi_{y(\max)}$ ($^\circ$), which are to be optimized. In the block of decision variables these values are described by extreme nodes D_{\min} and D_{\max} . During the optimization process, the computer randomly selected from a given block any nodes D_i (t_i , $\varphi_{x(i)}$, $\varphi_{y(i)}$) and remembered only those of them, which met all the limiting conditions. The node best describing the objective function represents optimal cell dimensions. A similar Monte-Carlo optimization algorithm was presented in Peliński and Smardzewski (2019).

The input data for the Monte-Carlo optimization function were comprised of the following values: $t_{\min} = 2.0$ mm, $t_{\max} = 5.0$ mm, $\varphi_{x(\min)} = 25^\circ$, $\varphi_{x(\max)} = 65^\circ$, $\varphi_{y(\min)} = 25^\circ$, $\varphi_{y(\max)} = 65^\circ$, and E_s (MPa) as given in Table 1 (for LayWood 40%). Adopting the number of sampling $N_0 = 30000$, the optimization process was completed, as the result of samplings was not improved. On this basis, four additional cells were selected, as presented in Fig. 5, in which the representative numerical values are given in Table 2.

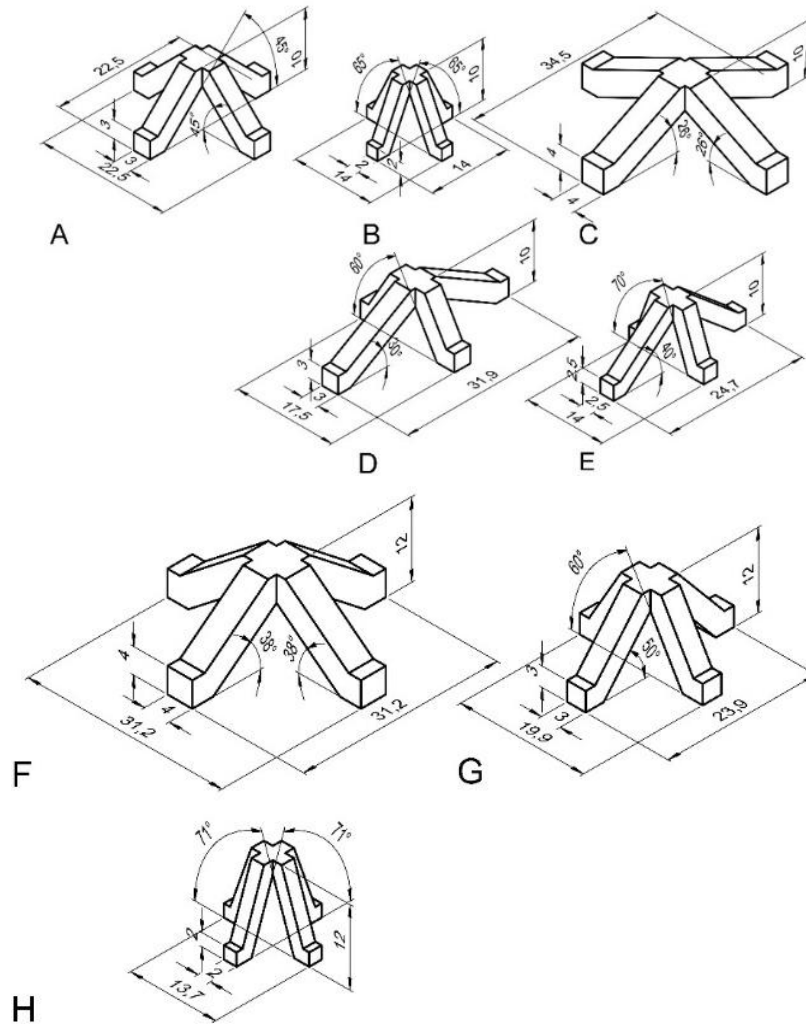


Fig. 4. Geometry of selected core cells: For models A to E $h = 10$ mm and for models F to H $h = 12$ mm, all units in mm

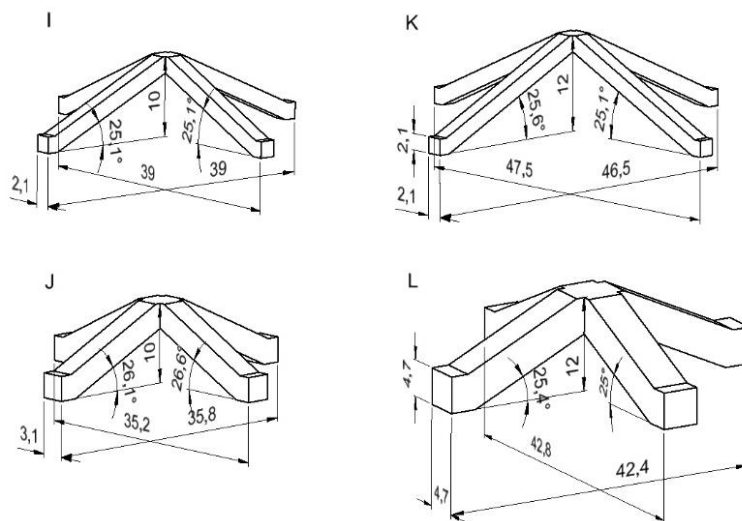


Fig. 5. Geometry of optimized cells: For models I to J $h = 10$ mm and for models K to L $h = 12$ mm, all units in mm

Table 2. Characteristic Properties of Selected Pyramidal Cells. LayWood 40% Filament

Cell Type	$2a = t$ mm	h	φ_x	φ_y	L_x	L_y	ρ	E_x	E_y	G_{xy}
			($^\circ$)		(mm)			(MPa)		
A	3.0	10	45	45	22.49	22.49	0.09936	11.52		5.76
B	2.0	10	65	65	14.01	14.01	0.09764	1.82		0.91
C	4.0	10	26	26	34.45	34.45	0.09901	41.21		20.60
D	3.0	10	30	60	31.86	17.55	0.09739	11.54	11.01	5.77
E	2.5	10	40	70	24.70	13.96	0.09788	5.41	4.47	2.70
F	4.0	12	38	38	31.23	31.23	0.09907	18.44		9.22
G	3.0	12	50	60	23.90	19.86	0.09765	5.20	4.88	2.60
H	2.0	12	71	71	13.74	13.74	0.09802	0.79		0.39
Optimized Cells										
I	2.06	10	25.08	25.08	38.97	38.97	0.02361	2.65		1.32
J	3.12	10	26.08	26.60	35.79	35.19	0.05931	13.55	13.57	6.77
K	2.05	12	25.64	25.08	46.49	47.53	0.01625	1.35	1.35	0.67
L	4.67	12	25.36	25.04	42.37	42.79	0.09088	36.12	36.06	18.06

Numerical Models

To verify the quality of the analytical models, FEM computations were performed for pre-selected pyramidal cores, as presented in Table 2. In view of the diversity in cell-arm size, it was assumed that each core should contain at least three cells in both directions, X and Y . Thus, the formed models were used in the numerical analysis by the FEM analysis. An example of a computer model for a pyramidal core with cell A is presented in Fig. 6.

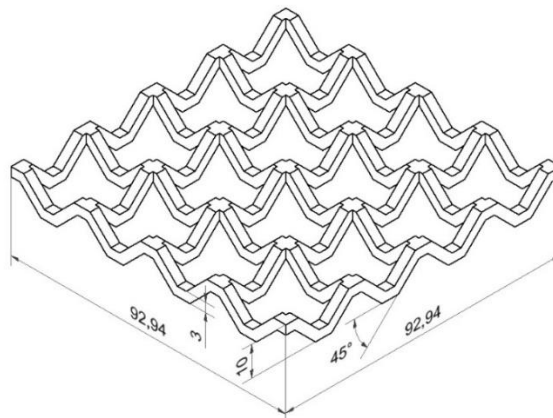


Fig. 6. A CAD (computer aided design) model for rib core type A, all units in mm

Calculations were performed using the Abaqus v.6.13 program (Dassault Systemes Simulia Corp., Waltham, MA, USA) and the EAGLE computing cluster (Poznań Supercomputing and Networking Center, PSNC, Poznan, Poland) within the computing grant "Properties of furniture panels with synclastic face and auxetic core". The computing model is presented in Fig. 7. The tetrahedral mesh was applied along with elastic-plastic strains for selected materials. The models had a mean number of nodes at 0.5 to 1.2 million and a mean number of elements at 0.3 to 1 million. Cubic elements C3D6 and C3D8R were used.

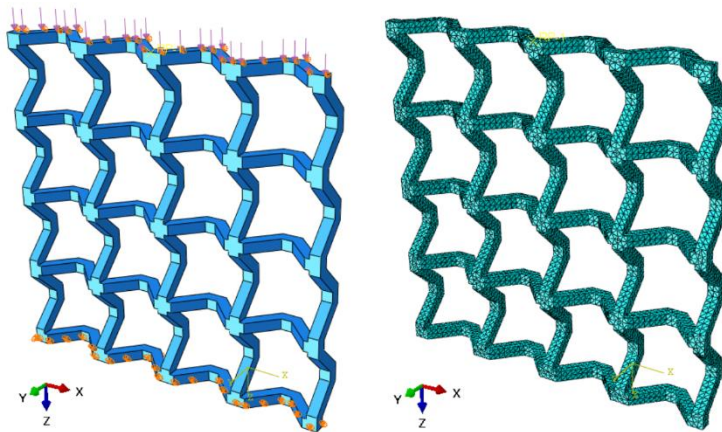


Fig. 7. An example model of the core used in numerical calculations

Computations were performed for loads in the direction of the X-axis and next the Y-axis, recording the respective elongations Δ_x and Δ_y (mm). Appropriate compressive loads were adopted at values from 0 N to 15 N at every 3 N for cells type G and H, from 0 N to 30 N at every 5 N for cells type B, I, J, K, and L, from 0 N to 60 N at every 10 N for cells type E and F, and from 0 N to 120 N at every 20 N for cells type A, C, and D. Loads were selected depending on rib thickness and their angle. The values of elastic constants obtained from numerical calculations are given in Table 3.

Experiment

It was decided to experimentally verify the results of analytical and numerical computations. For the purpose of this experiment, physical models of the core were constructed using 12 different pre-selected cell geometries. Three types of previously described filament types were applied in 3D printing. For each geometry type, five samples were prepared, providing a total of 180 samples (Figs. 8 and 9).

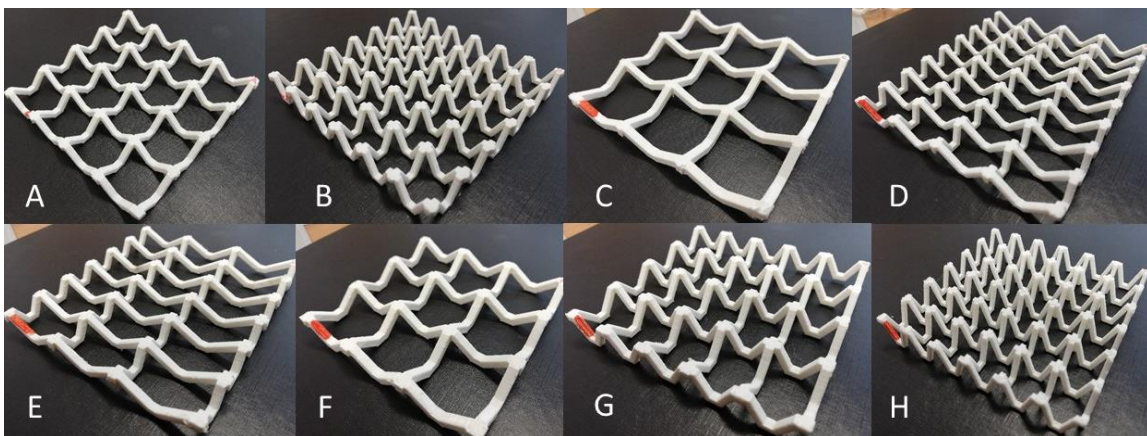


Fig. 8. Models of pyramidal cell cores A to H

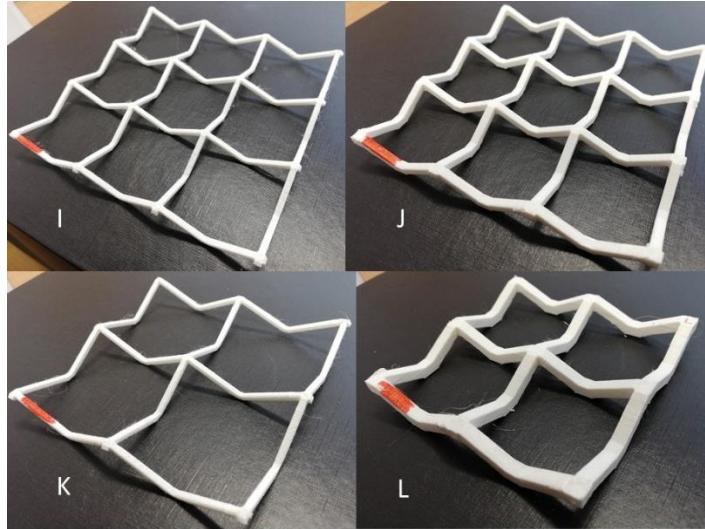


Fig. 9. Models of pyramidal cell cores I to L

The core was manufactured using a 3D M200 printer (Zortrax, Olsztyn, Poland) with a printing nozzle diameter of 0.2 mm. During 3D printing, the nozzle temperature was kept at 240 °C for LayWood and 190 °C for PLA. The thickness of a single printed layer ranged from 0.14 mm to 0.19 mm, depending on the core type. The temperature of the printer platen was 50 °C for all the materials and core types. The average printing time for a single sample was 4 h.

To determine the elastic properties of printed cores, the tests were performed using the specially designed instrumentation. A similar experimental test was reported by Peliński and Smardzewski (2019). The diagram of a testing station with a sample loaded with F (N) is presented in Fig. 10.

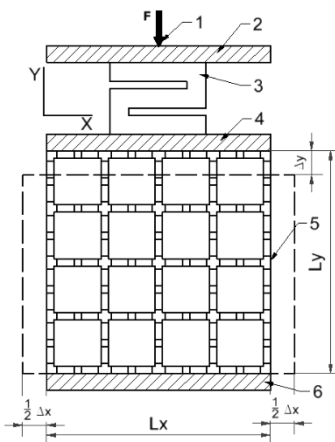


Fig. 10. The testing station: 1 - Press bolt; 2 - Sensor pressure plate; 3 - Strain gauge; 4 - Sample plate; 5 - Sample; and 6 - Support

The testing station was composed of a support beam (6), on which a sample was placed, and plates (2 and 4) between which a strain gauge (3) (ZEMIC H3-C3-25kg-3B, Serial No. P2Z122353; Zemic, Hanzhong, China) recorded the force exerted on the tested core accurate to 0.001 N. The station was lighted using two lamps of 630 lumens. The

samples were tested following the described methodology. For each applied load, a monochromatic picture was taken with an Olympus OM-D camera (Olympus, Tokyo, Japan). Next, the core strain was analyzed using the National Instruments IMAQ Vision Builder 6.1 linear analysis software (National Instruments, Austin, TX, USA) (Fig. 11).

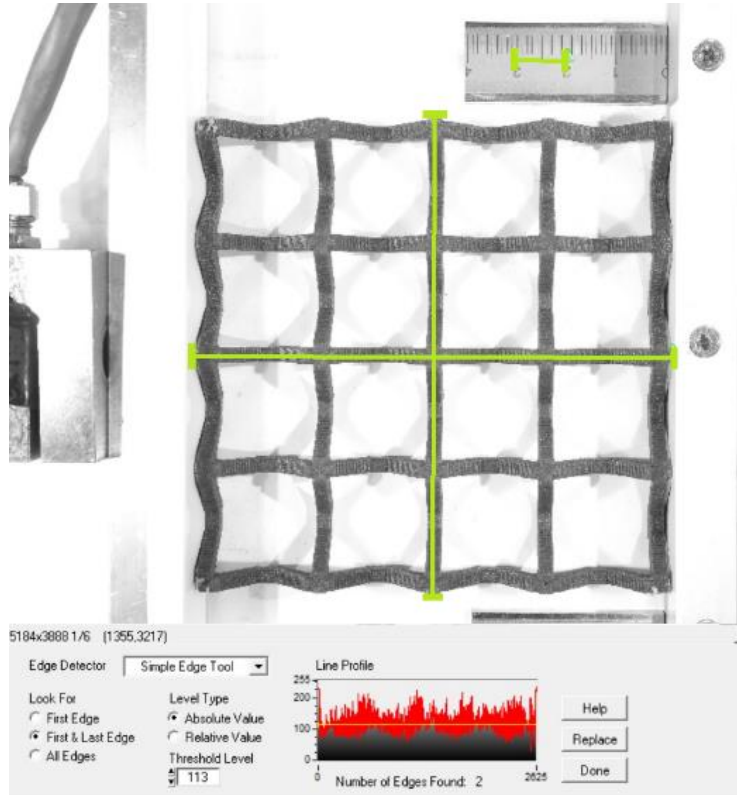


Fig. 11. Measurement of core strains

Applying the edge detection method in the digital image analysis, Poisson's ratios and moduli of linear elasticity were calculated from the following dependencies (Eqs. 21 to 24),

$$v_{yx} = \frac{\Delta_x \cdot L_y}{L_x \cdot \Delta_y} \text{ for direction } Y \quad (21)$$

$$v_{xy} = \frac{\Delta_y \cdot L_x}{L_y \cdot \Delta_x} \text{ for direction } X \quad (22)$$

$$E_y = \frac{F_y \cdot L_y}{h \cdot L_x \cdot \Delta_y} \text{ for direction } Y \quad (23)$$

$$E_x = \frac{F_x \cdot L_x}{h \cdot L_y \cdot \Delta_x} \text{ for direction } X \quad (24)$$

where $F_{(x \text{ or } y)}$ (N) is loading for directions X and Y .

Following the image analyses, elastic constants were determined for the tested cores and are given in Table 3.

Results of experimental tests were analyzed statistically by applying an analysis of variance (ANOVA) with multivariate classification. First, it was decided to determine the significance of the effect of core material type (M) and type of core cells (TC) on their moduli of linear elasticity (E). It was also decided to establish the significance of the M *

TC interaction. In the course of further statistical analyses, the differences between means from individual groups were investigated. For this purpose, Tukey's test (HSD) was applied. To show the significance of the quality of results obtained from numerical calculations and experimental testing a Student's t-test was used. All the computations were performed with the Statistica 13.1 software (StatSoft Polska Sp. z o.o., Kraków, Poland).

RESULTS AND DISCUSSION

It was initially decided to compare the results of analytical computations for moduli of elasticity given in Table 2 with the results of numerical calculations presented in Table 3. A preliminary review of the obtained data indicated that the values from analytical computations were two times overestimated in relation to the numerical calculations. This was directly caused by the analysis of a single cell considering solely the bending of its arms. While the presented analytical models idealized core cell structures, they nevertheless facilitated the prediction of relationships between its parameters. They were also effective in selecting 12 specific structures for further numerical and experimental studies.

When analyzing the results of numerical calculations from Table 3, a significant effect of the angle of rib arms on the modulus of linear elasticity in the core was observed. The modulus of linear elasticity E_x and E_y (MPa) decreased with an increase in angles φ_x and φ_y ($^\circ$). Other significant parameters affecting the mechanical properties of pyramidal cores were connected with thickness t (mm) and width of rib base $2a$ (mm). These regularities were observed at uniform relative density of all tested cores.

When investigating the results of experimental studies in Table 3, it was decided to first describe the dependencies between the moduli of linear elasticity for pyramidal cores manufactured from PLA. The review of this analysis showed the greatest modulus of linear elasticity $E_x = 24.19$ MPa for the core composed of F-type cells. This core consisted of cells with a transverse cross-sectional area of 16 mm^2 inclined at an angle $\varphi_x = \varphi_y = 38^\circ$. Cell F has Poisson's ratio $\nu_{xy} = \nu_{yx} = 0.101$ and relative density of 0.09907. Similar values are given for the truss core with C-type cells, in which the arm cross-section was identical to that of F cells. It only varied in angle $\varphi_x = \varphi_y = 26^\circ$ with the modulus of linear elasticity $E_x = 19.62$ MPa. Cores characterized by similar transverse sections and arm angles have moduli of linear elasticity ranging from 5 MPa to 20 MPa. In turn, the cells with a transverse section area of maximum 6.25 mm^2 (types B, G, H, I, and K) and arm angle ranging from 55° to 70° had the lowest values of moduli of linear elasticity ranging from 0.3 MPa to 4 MPa. The described differences in the results may have been caused, among other things, by geometrical imperfections of manufactured cores. The imperfections developed as a result of the structural material being deposited layer-by-layer. For an arm with a section area of 4 mm^2 for the deposited layer thickness of 0.14 mm, the accuracy of deposition and filling of a single material layer was maximum at 93%. In turn, for the core with the arm transverse section area of 16 mm^2 and layer thickness of 0.19 mm this accuracy was 95%.

Among cores manufactured from LayWood 40% (LB) the highest modulus of linear elasticity $E_x = 14.73$ MPa and Poisson's ratio $\nu_{xy} = 0.070$ were recorded for the core with C-type cells. Among cores manufactured from LayWood 30% (LY) the highest

modulus of linear elasticity $E_x = 17.82$ MPa and Poisson's ratio $\nu_{xy} = 0.072$ were recorded for the core with F-type cells.

Table 3. Results of FEM Analyses and Experimental Tests

Cell Type	Material Type	Numerical Models Results				Experimental Test Results			
		E_x	E_y	ν_{xy}	ν_{yx}	E_x	E_y	ν_{xy}	ν_{yx}
		(MPa)		-		(MPa)		-	
A	PLA	6.154		0.045		6.033		0.055	
	LB	5.099		0.047		4.860		0.032	
	LY	4.598		0.039		4.454		0.047	
B	PLA	1.643		0.058		1.594		0.039	
	LB	0.545		0.052		0.679		0.058	
	LY	0.738		0.055		0.805		0.043	
C	PLA	19.617		0.077		20.899		0.063	
	LB	11.965		0.091		14.726		0.070	
	LY	12.790		0.065		14.680		0.058	
D	PLA	4.653	0.980	0.076	0.065	4.852	1.060	0.075	0.073
	LB	2.241	0.765	0.090	0.780	3.185	0.814	0.080	0.063
	LY	3.519	0.823	0.094	0.710	3.868	0.874	0.080	0.077
E	PLA	8.708	3.714	0.092	0.071	8.355	3.828	0.082	0.076
	LB	5.263	1.070	0.070	0.044	7.684	1.628	0.066	0.040
	LY	5.509	1.957	0.092	0.116	6.605	2.003	0.071	0.100
F	PLA	22.044		0.122		24.190		0.101	
	LB	10.992		0.128		12.735		0.131	
	LY	18.478		0.081		17.842		0.072	
G	PLA	1.257	1.965	0.047	0.049	1.072	2.082	0.051	0.064
	LB	0.606	0.847	0.032	0.042	0.452	0.754	0.025	0.034
	LY	1.022	1.466	0.042	0.069	1.030	1.494	0.038	0.056
H	PLA	0.800		0.058		0.681		0.054	
	LB	0.328		0.038		0.354		0.027	
	LY	0.466		0.059		0.522		0.060	
I	PLA	3.056		0.081		3.179		0.059	
	LB	0.433		0.065		0.556		0.073	
	LY	0.769		0.085		1.047		0.054	
J	PLA	7.110	5.354	0.076	0.092	7.736	5.747	0.077	0.048
	LB	2.474	1.732	0.102	0.115	2.375	1.825	0.105	0.080
	LY	4.167	6.121	0.099	0.099	1.920	6.700	0.088	0.091
K	PLA	1.116		0.265		1.124		0.340	
	LB	0.236		0.139		0.313		0.197	
	LY	0.384		0.149		0.423		0.240	
L	PLA	9.465		0.154		9.880		0.195	
	LB	5.081		0.099		5.084		0.133	
	LY	8.761		0.098		8.028		0.160	

When comparing these results of numerical analysis with experimental data given in Table 3, it was clear that they were comparable. Experimental tests of the core with F-type cells made from PLA had the mean modulus of linear elasticity $E_x = 24.19$ MPa, which was 9.74% higher than the result of numerical calculations for that cell. Poisson's ratios for that core differed 17.2%. For LB filaments and C cells these differences amounted to 14.8% and 23%, respectively. For LY filaments and F-type core the difference between moduli of linear elasticity was 3.44%, while between their Poisson's ratios it was 11.11%. The presented values indicated that numerical models were correct and described ideal structures, with no geometric imperfections. The imperfections in printed structures were the primary cause for the variation in experimental data and calculated FEM values.

Statistical Analysis

Table 4 presents the results of ANOVA for the effect of individual variables and their interactions on the values of the modulus of linear elasticity. The results from the data revealed that the effect of all variables was statistically significant.

Table 4. Results of ANOVA

Symbol	SS	DF	MS	F	p
	5715.127	1	5715.127	3967.491	0.00
M	441.165	2	220.583	153.130	0.00
TC	7083.204	15	472.214	327.815	0.00
M*TC	855.768	30	28.526	19.803	0.00
Error	326,991	227	1,440		

SS - Sum of squares, DF - degrees of freedom, MS - mean sum square, F – test value, P – level of probability

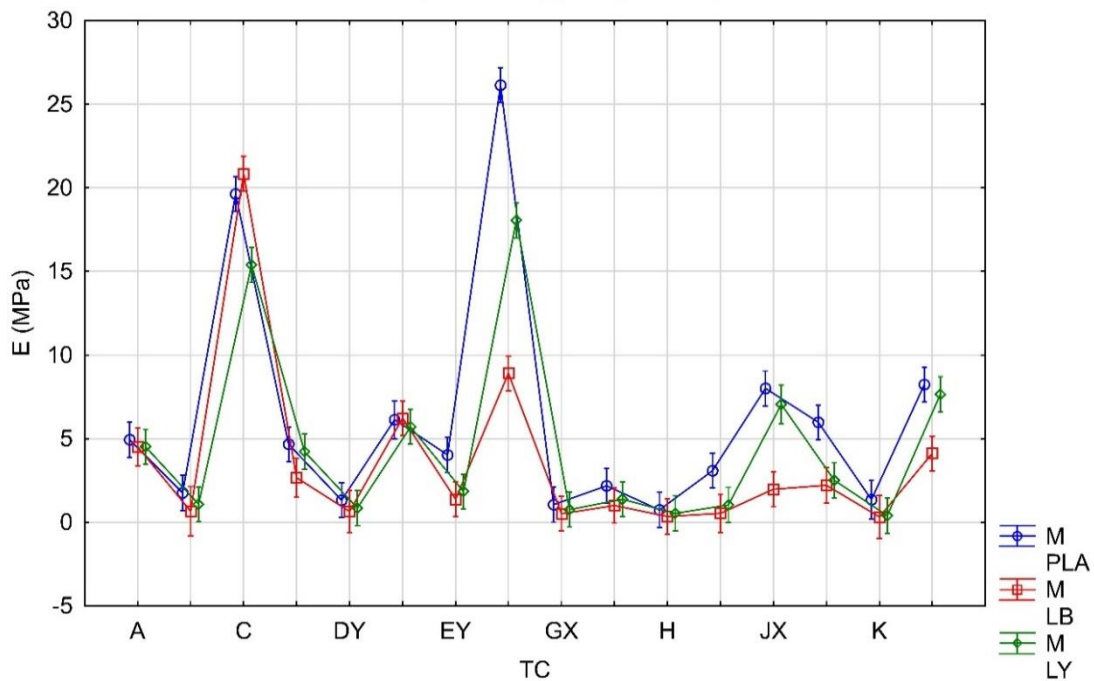


Fig. 12. Tukey's test for the effect of core type and type of material on modulus of linear elasticity E (MPa) in the core

The results from the ANOVA for the data given above showed that the type of material (M) had a significant effect on the modulus of linear elasticity for pyramidal cores. The strongest and the most significant effect of the type of core cell geometry (TC) on the modulus of linear elasticity was also evident. Additionally, the interaction between the material and type of cell core geometry (M * TC) had a significant effect on the modulus of linear elasticity for the pyramidal core (Fig. 12).

Figure 12 shows that for C-type and F-type cells, the effect of material type on the modulus of linear elasticity E (MPa) in the core was most significant. With an increase in values of elastic properties for a given material, particularly PLA, the greatest increase in moduli of linear elasticity for the cells was observed. This dependence indicated that the greatest sensitivity of C-type and F-type cells was to changes in the type of used material.

In the next step, it was decided to show the significance of quality in numerical and experimental results. Student's t-test was conducted to confirm this significance. Example values of Student's t-test for PLA are given in Table 5.

Table 5. Results of Student's t-test for Independent Samples, PLA

	Mean Group 1	Mean Group 2	t	df	p
A EXP vs. A FEM	4.93736	6.15385	-1.498	5	0.194489
B EXP vs. B FEM	1.75693	1.64258	1.209	5	0.280625
C EXP vs. C FEM	19.62118	19.61746	0.002	5	0.998684
DX EXP vs. DX FEM	4.66586	4.65279	0.014	5	0.989161
DY EXP vs. DY FEM	1.32261	0.98000	4.647	5	0.005596
EX EXP vs. EX FEM	6.13559	8.70827	-1.696	4	0.165184
EY EXP vs. EY FEM	4.02799	3.71405	0.241	5	0.819290
F EXP vs. F FEM	26.13480	22.04440	0.786	5	0.467407
GX EXP vs. GX FEM	1.06041	1.25686	-2.823	5	0.036982
GY EXP vs. GY FEM	2.17906	1.96502	0.491	5	0.644028
H EXP vs. H FEM	0.74419	0.80000	-0.795	5	0.462729
I EXP vs. I FEM	3.08794	3.05572	0.057	5	0.956432
JX EXP vs. JX FEM	8.00623	7.10968	3.458	5	0.018083
JY EXP vs. JY FEM	5.97875	5.35400	0.370	5	0.726702
K EXP vs. K FEM	1.35624	1.11607	2.446	4	0.070732
L EXP vs. L FEM	8.23326	9.46539	-1.224	5	0.275497

It may be concluded from the results presented in Table 5 that values of modulus of linear elasticity provided by the numerical analyses and the experimental tests did not differ significantly. Nevertheless, there were cells for which the difference in the results was significant. The cell-D in the Y direction, cell-G in the X direction, and cell-J in the X direction showed significant differences in the results obtained from the experimental tests and numerical analyses.

A Student's t-test was also performed for the other materials. For LB filaments, significant differences between the results of experimental tests and numerical analyses were found only for G-type cells in the X direction and for L-type cells. For LY filaments, differences between experimental data and numerical results were shown for type-B cells as well as type-G cells in the X direction. In all cases, these differences were explained by imperfections in geometry.

CONCLUSIONS

1. Among the investigated geometries of pyramidal cores, the greatest moduli of linear elasticity were obtained for cores type C, F, and L for all types of used filaments.
2. The best elastic properties were found in cells manufactured from polylactide (PLA), followed by those from LB and LY (with LayWood).
3. Cell geometry had a significant effect on elastic properties of cell cores while identical relative density of these structures was maintained. The angle of arms in the pyramidal cell had a particularly strong effect on these properties.
4. Geometrical imperfections had a considerable effect on the results of experimental tests.
5. Results of numerical analyses and the experimental test did not differ significantly. This confirmed the advisability of numerical analyses in future model studies.
6. Idealized analytical models showed very high differences in comparison to experimental tests and numerical simulations. Nevertheless, they make it possible to estimate dependencies between cell parameters.

ACKNOWLEDGMENTS

This study was funded from the National Science Centre NCN (Poland), project no. 2016/21/B/ST8/01016.

Computations were made using the EAGLE computing cluster at the Poznań Supercomputing and Networking Center within the computing grant "Properties of furniture panels with synclastic face and auxetic core".

REFERENCES CITED

- Alderson, A., and Alderson, K. (2007). "Auxetic materials," *International Journal for Trends in Engineering & Technology*, 5(2), 156-160. DOI: 10.1243/09544100JAERO185
- Barboutis, I., and Vassiliou, V. (2005). "Strength properties of lightweight paper honeycomb panels for the furniture," in: *10th Int. Sci. Conf. Eng. Des. Interior Furnit. Des.* pp. 17–18.
- Che, L., Xu, G., Zeng, T., Cheng, S., Zhou, X., and Yang, S. (2014). "Compressive and shear characteristics of an octahedral stitched sandwich composite," *Composite Structures* 112, 179–187. DOI: 10.1016/j.compstruct.2014.02.012
- Chen, Z., and Yan, N. (2012). "Investigation of elastic moduli of kraft paper honeycomb core sandwich panels," *Composites Part B: Engineering* 43(5), 2107-2114. DOI: 10.1016/j.compositesb.2012.03.008
- Finnegan, K., Kooistra, G., Wadley, H. N. G., and Deshpande, V. S. (2007). "The compressive response of carbon fiber composite pyramidal truss sandwich cores," *International Journal of Materials Research* 98(12), 1264-1272. DOI: 10.3139/146.101594
- Gao, L., Sun, Y., Cong, L., and Chen, P. (2013). "Mechanical behaviours of composite

- sandwich panel with strengthened pyramidal truss cores,” *Composite Structures* 105, 149-152. DOI: 10.1016/j.compstruct.2013.05.015
- He, Z. Z., Wang, F. C., Zhu, Y. B., Wu, H. A., and Park, H. S. (2017). “Mechanical properties of copper octet-truss nanolattices,” *Journal of the Mechanics and Physics of Solids* 101(January), 133–149. DOI: 10.1016/j.jmps.2017.01.019
- Imbalzano, G., Tran, P., Ngo, T. D., and Lee, P. V. S. (2016). “A numerical study of auxetic composite panels under blast loadings,” *Composite Structures* 135, 339-352. DOI: 10.1016/j.compstruct.2015.09.038
- Jin, M., Hu, Y., and Wang, B. (2015). “Compressive and bending behaviours of wood-based two-dimensional lattice truss core sandwich structures,” *Composite Structures* 124, 337-344. DOI: 10.1016/j.compstruct.2015.01.033
- Klimek, P., Wimmer, R., Brabec, M., and Sebera, V. (2016). “Novel sandwich panel with interlocking plywood kagome lattice core and grooved particleboard facings,” *BioResources* 11(1), 195-208. DOI: 10.15376/biores.11.1.195-208
- Loinsigh, C. O., Oudjene, M., Shotton, E., Pizzi, A., and Fanning, P. (2012). “Mechanical behaviour and 3D stress analysis of multi-layered wooden beams made with welded-through wood dowels,” *Composite Structures* 94(2), 313-321. DOI: 10.1016/j.compstruct.2011.08.029
- Majewski, A., and Smardzewski, J. (2012). “Thin purenit honeycomb panels,” in: *XXVth International Conference Research for Furniture Industry*, Poznań, Poland, September 19-20th 2013, 63-72.
- Peliński, K., and Smardzewski, J. (2019). “Experimental testing of elastic properties of paper and WoodEpoX® in honeycomb panels,” *BioResources* 14(2), 2977-2994. DOI: 10.15376/biores.14.2.2977-2994
- PN-EN ISO 527-3 (1998). Tworzywa sztuczne - Oznaczenie właściwości mechanicznych przy statycznym rozciąganiu - Warunki badań folii i płyt.
- Sam-Brew, S., Semple, K., and Smith, G. D. (2011). “Preliminary experiments on the manufacture of hollow core composite panels,” *Forest Products Journal* 61(5), 381-389. DOI: 10.13073/0015-7473-61.5.381
- Schneider, C., Velea, M. N., Kazemahvazi, S., and Zenkert, D. (2015). “Compression properties of novel thermoplastic carbon fibre and poly-ethylene terephthalate fibre composite lattice structures,” *Materials and Design* 65(September), 1110-1120. DOI: 10.1016/j.matdes.2014.08.032
- Smardzewski, J. (2013). “Elastic properties of cellular wood panels with hexagonal and auxetic cores,” *Holzforschung* 67(1). DOI: 10.1515/hf-2012-0055
- Smardzewski, J. (2015). “Mechanical properties of wood-based sandwich panels with a wavy core,” in: *XXVII International Conference Research for Furniture Industry*, September 17th - 18th 2015, Gazi University, Ankara, Turkey, 242-255.
- Smardzewski, J., and Jasińska, D. (2016). “Mathematical models and experimental data for HDF based sandwich panels with dual corrugated lightweight core,” *Holzforschung* 71(3), 265-273. DOI: 10.1515/hf-2016-0146
- Smardzewski, J., and Majewski, A. (2015). “Mechanical properties of auxetic honeycomb core with triangular cells,” in: *25th International Scientific Conference New Materials and Technologies in the Function of Wooden Products*, 103-112.
- Smardzewski, J., and Prekrat, S. (2012). “Modelling of thin paper honeycomb panels for furniture,” in: *22th International Scientific Conference, Wood is Good – With Knowledge and Technology to a Competitive Forestry and Wood Technology Sector*, University of Zagreb, Faculty of Forestry, Zagreb, October 2, 179-186.

- Smardzewski, J., Wojciechowski, K. W., and Poźniak, A. (2018). “Auxetic lattice truss cores fabricated of LayWood,” *BioResources* 13(4), 8823-8838. DOI: 10.15376/biores.13.4.8823-8838
- Smardzewski, J., and Wojciechowski, W. K. (2019). “Response of wood-based sandwich beams with three-dimensional lattice core,” *Composite Structures* 216, 340-349. DOI: 10.1016/j.compstruct.2019.03.009
- Voth, C., and Yadama, V. (2010). “Sustainable lightweight wood-strand panels for building construction,” *Proceedings of the International Convention of Society of Wood Science and Technology and United Nations Economic Commission for Europe - Timber Committee*, 1-7.
- Wadley, H. N. G., Fleck, N. A., and Evans, A. G. (2003). “Fabrication and structural performance of periodic cellular metal sandwich structures,” *Composites Science and Technology* 63(16), 2331-2343. DOI: 10.1016/S0266-3538(03)00266-5
- Wang, B., Wu, L., Ma, L., Sun, Y., and Du, S. (2010). “Mechanical behavior of the sandwich structures with carbon fiber-reinforced pyramidal lattice truss core,” *Materials and Design* 31(5), 2659-2663. DOI: 10.1016/j.matdes.2009.11.061
- Wojnowska, M., Peliński, K., Maslej, M., Słonina, M., and Smardzewski, J. (2017). “Elastic properties of periodic core’s structures of multilayers furniture panels,” *Journal of Advanced Technology Sciences* 6(3), 1249-1263.
- Xiong, J., Ma, L., Wu, L., Wang, B., and Vaziri, A. (2010). “Fabrication and crushing behavior of low density carbon fiber composite pyramidal truss structures,” *Composite Structures* 92(11), 2695-2702. DOI: 10.1016/j.compstruct.2010.03.010
- Yang, L., Harrysson, O., West, H., and Cormier, D. (2015). “Mechanical properties of 3D re-entrant honeycomb auxetic structures realized via additive manufacturing,” *International Journal of Solids and Structures*. DOI: 10.1016/j.ijsolstr.2015.05.005
- Yin, S., Wu, L., Ma, L., and Nutt, S. (2011). “Pyramidal lattice sandwich structures with hollow composite trusses,” *Composite Structures* 93(12), 3104-3111. DOI: 10.1016/j.compstruct.2011.06.025
- Yin, S., Wu, L., and Nutt, S. (2013). “Stretch-bend-hybrid hierarchical composite pyramidal lattice cores,” *Composite Structures*, 98, 153–159. DOI: 10.1016/j.compstruct.2012.11.004
- Zhang, G., Wang, B., Ma, L., Xiong, J., and Wu, L. (2013). “Response of sandwich structures with pyramidal truss cores under the compression and impact loading,” *Composite Structures* 100, 451-463. DOI: 10.1016/j.compstruct.2013.01.012
- Zhong, S., Guo, L., Lu, H., and Zeng, T. (2015). “A continuum damage model for three-dimensional woven composites and finite element implementation,” *Composite Structures* 128, 1-9. DOI: 10.1016/j.compstruct.2015.03.030

Article submitted: July 8, 2019; Peer review completed: September 8, 2019; Revised version received and accepted: September 16, 2019; Published: October 23, 2019.
DOI: 10.15376/biores.14.4.9686-9703